



## Probing NiO nanocrystals by EXAFS spectroscopy

A. Anspoks\*, A. Kuzmin, A. Kalinko, J. Timoshenko

*Institute of Solid State Physics, University of Latvia, Kengaraga street 8, LV-1063 Riga, Latvia*

### ARTICLE INFO

#### Article history:

Received 13 July 2010

Accepted 21 September 2010

by E.L. Ivchenko

Available online 27 September 2010

#### Keywords:

A. Nanostructures

C. EXAFS

C. Crystal structure and symmetry

### ABSTRACT

The structure relaxation in nanocrystalline NiO (nano-NiO, 13 nm crystallite size) has been studied by X-ray absorption spectroscopy at the Ni K-edge at 300 K. Conventional single-scattering analysis of the EXAFS signals from the first two coordination shells showed a lattice volume expansion by about 1% and a contraction of the Ni–O bonds by about 0.5% in nano-NiO compared to microcrystalline NiO. A more sophisticated approach, based on a combination of classical molecular dynamics and ab initio multiple-scattering EXAFS theory, allowed us to interpret both static relaxation and lattice dynamics in nano-NiO.

© 2010 Elsevier Ltd. All rights reserved.

### 1. Introduction

The chemical and physical properties of nanoparticles are determined by their shape and size. The difference between a nanoparticle and its bulk counterpart is caused by the large fraction of under-coordinated atoms at the surface and a consequent modification of the interatomic interactions [1]. A reduction in size of the nanoparticles is generally followed by an atomic structure relaxation, leading to compression or expansion of the nanoparticle volume. Volume compression is common for metal nanoparticles, whereas expansion is observed in most nano-metal-oxides [2–6]. In particular, lattice expansion has been observed recently by X-ray diffraction [7,8] in nanocrystalline NiO with a size below ~30 nm.

Among the different experimental methods, scattering techniques (as diffraction and PDF analysis) and X-ray absorption spectroscopy are two probes which are widely used and yield direct information on the atomic structure of nanomaterials [9]. X-ray absorption spectroscopy (XAS), being sensitive to the local environment around absorbing center, is complementary to scattering techniques and has some advantages due to atom type and site selectivity, sensitivity to high dilutions (low concentration) and to many-atom distribution functions through the so-called multiple-scattering (MS) contributions [10,11]. Besides, XAS gives not only bulk averaged structural information but can provide spatially resolved data at the nano-scale when combined with scanning probe microscopy (SPM) used as a local nano-probe [12–14].

Although a reliable theory of X-ray absorption spectra (EXAFS, extended X-ray absorption fine structure) is currently available [11,15] and allows relatively simple analysis of the first coordination shell contribution [16,17], the extraction of structural information from the outer coordination shells of absorbing atoms remains a challenge.

In this work we report on the original study of the structure relaxation and lattice dynamics in nanocrystalline NiO by Ni K-edge X-ray absorption spectroscopy using the conventional single-scattering approach [16,17] and a recently developed advanced method [18], based on the combined use of classical molecular dynamics and ab initio multiple-scattering EXAFS theory.

### 2. Experimental and data analysis

The black NiO nanoparticles (nano-NiO) were produced by a precipitation method [19], based on a reaction of aqueous solutions of  $\text{Ni}(\text{NO}_3)_2 \cdot 6\text{H}_2\text{O}$  and NaOH with subsequent annealing in air at 250 °C. Their average size was 13 nm, according to the BET specific surface area measurements. Commercial green microcrystalline nickel oxide powder (c-NiO, Aldrich, 99%) was used for comparison.

The Ni K-edge EXAFS signals were measured in transmission mode at the HASYLAB DESY C1 bending-magnet beamline at 300 K. The storage ring DORIS III operated at  $E = 4.44$  GeV and  $I_{\text{max}} = 140$  mA. The X-rays were monochromatized by a 40% detuned Si(111) double-crystal monochromator, and the beam intensity was measured using two ionization chambers filled with argon and krypton gases. The powder samples were deposited on Millipore filters and fixed by Scotch tape.

The X-ray absorption spectra were analyzed using the “EDA” software package [16]. The extended X-ray absorption fine structure (EXAFS) signals were extracted following the conventional

\* Corresponding author.

E-mail addresses: [aanspoks@cfi.lu.lv](mailto:aanspoks@cfi.lu.lv) (A. Anspoks), [a.kuzmin@cfi.lu.lv](mailto:a.kuzmin@cfi.lu.lv) (A. Kuzmin).

URL: <http://www.cfi.lv> (A. Anspoks).

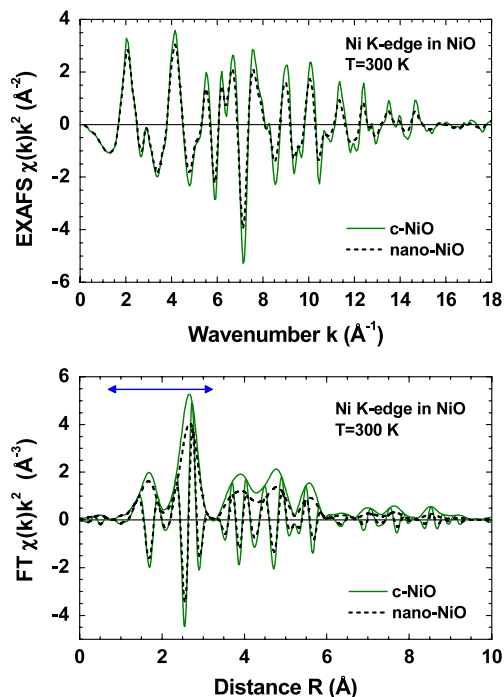


**Fig. 1.** Experimental Ni K-edge EXAFS  $\chi(k)k^2$  signals and their Fourier transforms for c-NiO (solid lines) and nano-NiO (dashed lines) at 300 K.

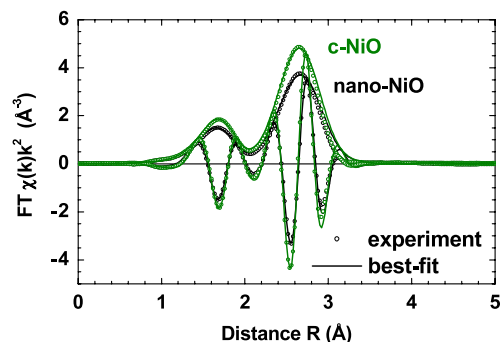


**Fig. 2.** Fourier transforms of the experimental (open circles) and calculated (solid lines) Ni K-edge EXAFS  $\chi(k)k^2$  signals for c-NiO and nano-NiO within the range of the first two ( $O_1$ ,  $Ni_2$ ) coordination shells.

procedure [17] and are shown in Fig. 1. Note the high quality of obtained EXAFS data in a wide  $k$ -space range up to  $18 \text{ \AA}^{-1}$ . As a result, a set of structural peaks is clearly visible above the noise level in the Fourier transforms (FTs) of the EXAFS signals up to  $\sim 9.5 \text{ \AA}$ . A comparison of the FT shapes for c-NiO and nano-NiO samples indicates the typical behavior for nanosized compounds, i.e. a reduction of the peak amplitudes upon an increase of the distance, with the peak position remaining nearly unchanged.

The EXAFS signals were analyzed using two methods: (i) a conventional multi-component approach within the single-scattering approximation [17], and (ii) a recently developed MD-EXAFS approach, described in the next section and based on the use of classical molecular dynamics (MD) and ab initio multiple-scattering theory [18].

In the conventional analysis, the contributions from the first two coordination shells ( $Ni-O_1$  and  $Ni-Ni_2$ ) were isolated by the Fourier filtering method in the  $R$ -space range of  $0.7\text{--}3.2 \text{ \AA}$  and best-fitted in the  $k$ -space range of  $2\text{--}15 \text{ \AA}^{-1}$  using the two-component Gaussian model in the single-scattering approximation [16]. The amplitude and phase shift functions for the  $Ni-O$  and  $Ni-Ni$  atom pairs used in the fits were calculated by the FEFF8 code [20]. The

**Table 1**

Structural parameters for the first and second coordination shells in c-NiO and nano-NiO obtained from the best-fit of the EXAFS signals.

	1 shell ( $Ni-O_1$ )	2 shell ( $Ni-Ni_2$ )
c-NiO		
$N$	$6 \pm 0.2$	$12 \pm 0.4$
$R$ ( $\text{\AA}$ )	$2.070 \pm 0.003$	$2.949 \pm 0.003$
$\sigma^2$ ( $\text{\AA}^2$ )	$0.0057 \pm 0.0005$	$0.0067 \pm 0.0005$
nano-NiO		
$N$	$5.8 \pm 0.2$	$11.3 \pm 0.4$
$R$ ( $\text{\AA}$ )	$2.061 \pm 0.003$	$2.961 \pm 0.003$
$\sigma^2$ ( $\text{\AA}^2$ )	$0.0077 \pm 0.0005$	$0.0082 \pm 0.0005$

calculations were performed for a cluster of  $8 \text{ \AA}$  size centered at the absorbing Ni atom and having the cubic NiO structure [21]. The inelastic losses were taken into account using the complex exchange-correlation Hedin-Lundqvist potential [11]. The best-fit results are shown in Fig. 2, and the values of the coordination numbers ( $N$ ), the interatomic distances ( $R$ ) and the mean-squared relative displacements (MSRDs) ( $\sigma^2$ ) are given in Table 1.

### 3. MD-EXAFS simulations

To go beyond the limitations of the conventional EXAFS analysis, we employed a recently developed simulation method [18], based on the use of classical molecular dynamics (MD), to calculate configuration-averaged EXAFS signals for c-NiO and nano-NiO at  $T = 300 \text{ K}$ .

First, we performed NVT-type classical MD simulations using the GULP 3.1 code [22], which is suitable for both crystalline and nanosized materials. Crystalline c-NiO was modeled by the supercell  $6a_0 \times 6a_0 \times 6a_0$  ( $a_0 = 4.1773 \text{ \AA}$  [21] is the lattice parameter) with 3D periodic boundary conditions. The nanosized NiO was simulated by a cluster having the cubic shape and a size of up to  $6a_0 \times 6a_0 \times 6a_0$ ; no boundary conditions were employed in this case. Here only results for the largest size ( $6a_0 \times 6a_0 \times 6a_0$ ) are reported. Our estimate for the cubic shape particles indicates that the difference between a crystal and nanoparticle can be detected in the EXAFS signal for particle sizes smaller than about  $400 \text{ \AA}$ . For larger particles, the contribution from atoms located close to the surface and having reduced coordination becomes too small to be detectable. Currently, a size of about  $25 \text{ \AA}$  is the largest technically acceptable in our simulations and provides the EXAFS signal being in the closest agreement with the experimental one.

The force-field (FF) potential model included two-body central force interactions described by a sum of the Buckingham and Coulomb potentials

$$U_{ij}(r_{ij}) = A_{ij} \exp\left(-\frac{r_{ij}}{\rho_{ij}}\right) - \frac{C_{ij}}{r_{ij}^6} + \frac{Z_i Z_j e^2}{r_{ij}}. \quad (1)$$

The Buckingham potential parameters ( $A$ ,  $\rho$ , and  $C$  in Table 2) were taken from previous simulations of c-NiO in [23,24]. The formal ion charges  $Z$  ( $Z = +2$  for Ni and  $Z = -2$  for O) were used in the Coulomb potential [23,24]. The integration of Newton's equations was performed by the leapfrog Verlet method [22]. In each simulation, the structure was first equilibrated during  $20 \text{ ps}$  at  $300 \text{ K}$ , corresponding to the temperature of the EXAFS experiments, and a set of instantaneous atomic configurations was accumulated during the  $20 \text{ ps}$  production run with a time step of  $0.5 \text{ fs}$ . The thus obtained sets of instantaneous atomic configurations were used to calculate the total and pair radial distribution functions (RDFs), which were then used to evaluate the values of MSRDs for the first and second shells.

Next, the Ni K-edge EXAFS signals were calculated for each instantaneous atomic configuration using the ab initio FEFF8

**Table 2**  
Parameters of the Buckingham potentials for c-NiO and nano-NiO.

Pair of atoms	$A$ (eV)	$\rho$ (Å)	$C$ (eV Å <sup>6</sup> )
c-NiO [23]			
Ni <sup>+2</sup> -O <sup>-2</sup>	754.92	0.3277	0.0
O <sup>-2</sup> -O <sup>-2</sup>	22764.3	0.1490	27.89
c-NiO [24]			
Ni <sup>+2</sup> -O <sup>-2</sup>	775.0	0.3250	0.0
O <sup>-2</sup> -O <sup>-2</sup>	22764.3	0.1490	20.37
nano-NiO			
Ni <sup>+2</sup> -O <sup>-2</sup>	754.92	0.3310	0.0
O <sup>-2</sup> -O <sup>-2</sup>	22764.3	0.1505	27.89

code [20]. The scattering potentials and partial phase shifts were evaluated only once for the average configuration, thus neglecting a variation of the scattering potentials due to thermal vibrations [18]. Multiple-scattering effects were taken into account up to the eighth order with the half path length up to 6.5 Å. The inelastic losses were taken into account using the complex exchange-correlation Hedin-Lundqvist potential [11]. The cluster potential was of the muffin-tin (MT) type, and the values of the MT-radii were  $R_{\text{MT}}(\text{Ni}) = 1.319$  Å and  $R_{\text{MT}}(\text{O}) = 1.021$  Å. The configuration-averaged EXAFS signal was obtained by averaging over several thousand configurations, and its convergence was controlled. All calculations were performed on the “LASC” cluster-type computer at ISSP (Riga) [25].

#### 4. Results and discussion

The Ni K-edge EXAFS signals for c-NiO and nano-NiO are rather similar except for the amplitude damping and a slight difference in the frequency of oscillations, both are better observed at high  $k$ -values (Fig. 1). The Fourier transforms (FTs) of the EXAFS signals demonstrate the progressive lowering of the peak amplitudes at longer  $R$ -values. Such behavior is typical for the manifestation of the nanosized effect in NiO [26]. However, the positions of the peaks in the FTs are close, suggesting a similarity in the local environment in the nanocrystals to that in c-NiO. In fact, the average lattice of nano-NiO is close to that in c-NiO [7,8].

Conventional analysis of the EXAFS signal from the first two peaks in the FTs (Fig. 1) has been performed within the single-scattering approximation taking into account contributions from the first and second coordination shells, composed of oxygen (O<sub>1</sub>) and nickel (Ni<sub>2</sub>) atoms, respectively. The very good agreement obtained between the calculated and experimental EXAFS signals (Fig. 2) gives us confidence in the values of the structural parameters ( $N, R, \sigma^2$ ) reported in Table 1. The coordination numbers and interatomic distances for c-NiO agree well with crystallographic values ( $N_{\text{XRD}}(\text{O}_1) = 6$ ,  $R_{\text{XRD}}(\text{Ni-O}_1) = 2.089$  Å, and  $N_{\text{XRD}}(\text{Ni}_2) = 12$ ,  $R_{\text{XRD}}(\text{Ni-Ni}_2) = 2.954$  Å [21]). As one can see, a decrease of the crystallite size in nano-NiO results in a detectable local structure variation. The average coordination numbers decrease due to the under-coordinated atoms located at the nanoparticle surface. In fact, it is expected [26] that the effect should be stronger for more distant coordination shells, as is observed in Fig. 1. The interatomic distances behave differently in the first and second shells: upon a decrease of crystallite size from c-NiO to nano-NiO, the Ni-O<sub>1</sub> distance decreases by 0.01 Å, whereas the Ni-Ni<sub>2</sub> increases by about the same amount. Besides, the MSRD values in both shells are larger in nano-NiO. These facts indicate that a relaxation of the local structure occurs in nano-NiO and is accompanied by an increase of disorder.

Comparing the total EXAFS signals in Fig. 1, one can observe that the phase difference of oscillations increases progressively from low to high wavenumber values in nano-NiO in comparison with c-NiO. This indicates that the average lattice parameter ( $a_0$ ) in nano-NiO is slightly larger than in c-NiO. Their values can be estimated

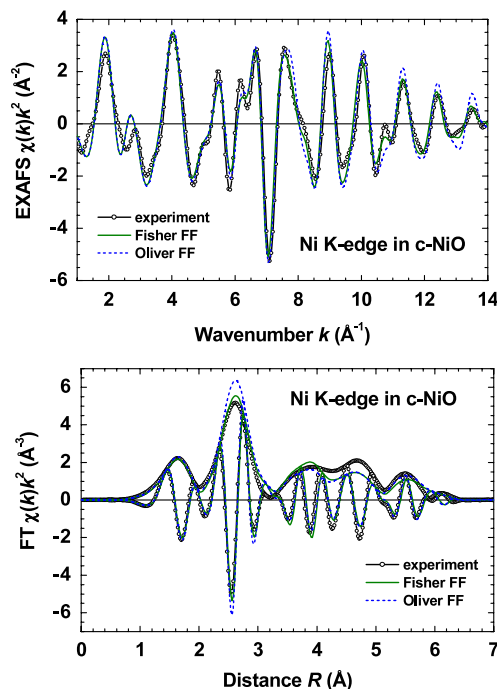


**Fig. 3.** Comparison of calculated (solid line – Fisher’s potential [23], dashed line – Oliver’s potential [24]) and experimental (open circles) Ni K-edge EXAFS  $\chi(k)k^2$  signals and their Fourier transforms for c-NiO.

from Ni-Ni<sub>2</sub> distances and are equal to  $a_0 = 4.188$  Å for nano-NiO and  $a_0 = 4.171$  Å for c-NiO ( $a_0 = 4.1773$  Å for c-NiO from X-ray diffraction [21]). Assuming the cubic shape for nanoparticles, one can estimate the change in the lattice volume to be  $V/V_0 \approx 1\%$  ( $V_0 = 72.54$  Å<sup>3</sup> for c-NiO and  $V = 73.43$  Å<sup>3</sup> for nano-NiO). A lattice expansion is typical for nanocrystalline oxides and has been observed recently by X-ray diffraction for NiO with crystallite sizes below 30 nm [7,8]. Note that our results agree well with those in [7,8].

To interpret the outer shell (beyond the second one) contributions to the total EXAFS signal, one must correctly take into account the multiple-scattering (MS) effects. This is especially important for NiO, where the highly symmetric cubic lattice gives rise to many linear MS paths with large relative amplitudes. The accurate solution of this problem is a challenge for current EXAFS data analysis. Here we address it through the calculation of the configuration-averaged EXAFS signal.

As a starting point, we performed simulations for crystalline nickel oxide (c-NiO) using two simple FF potential models, developed by Fisher [23] and Oliver [24] (Table 2), which reproduce rather well a number of NiO properties such as lattice constant, bulk modulus, elastic constants, and dielectric constants [23,24]. General agreement between configuration-averaged EXAFS signals calculated with the two potential models and experiment for c-NiO is good (Fig. 3), especially taking into account the simplicity of the models and the absence of any fitting parameter. However, Fisher’s model [23] provides slightly better agreement in the region of the second peak at 2.6 Å in the FT; therefore it was used further for the simulation of nanoparticle.

The configuration-averaged EXAFS signals for a nanoparticle having the  $6a_0 \times 6a_0 \times 6a_0$  size are shown in Fig. 4. The EXAFS signal, calculated using the original Fisher’s FF model [23], reproduces the amplitude of the experimental signal but fails to reproduce its frequency. Our conclusion is that it is not possible to transfer a phenomenological interaction potential from bulk material to nanosolid since, in addition to size reduction, a change

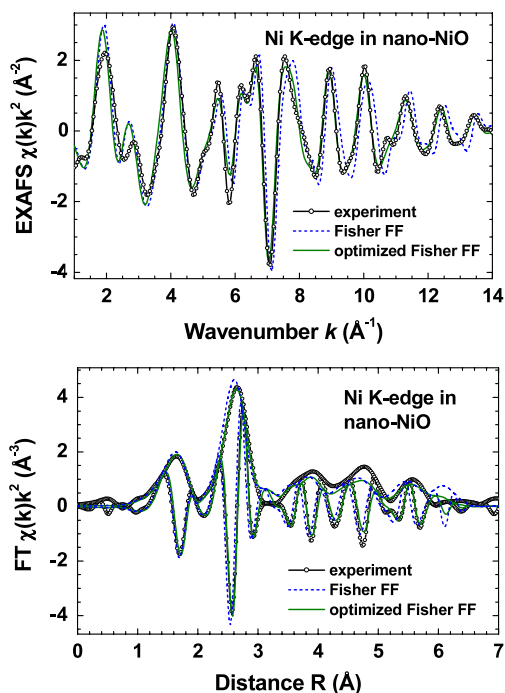


**Fig. 4.** Comparison of calculated (dashed line—Fisher's potential [23], solid line—optimized potential) and experimental (open circles) Ni K-edge EXAFS  $\chi(k)k^2$  signals and their Fourier transforms for nano-NiO.

**Table 3**

Structural parameters ( $N$  is the coordination number,  $R$  is the interatomic distance, and  $\sigma^2$  is the MSRD) for the first six coordination shells in c-NiO and nano-NiO obtained by decomposition of the Ni–O and Ni–Ni RDFs into Gaussian components.

	O <sub>1</sub>	Ni <sub>2</sub>	O <sub>3</sub>	Ni <sub>4</sub>	O <sub>5</sub>	Ni <sub>6</sub>
c-NiO						
$N$	6	12	8	6	24	24
$R$ (Å)	2.083	2.949	3.610	4.167	4.661	5.106
$\sigma^2$ (Å <sup>2</sup> )	0.0055	0.0042	0.0059	0.0056	0.0062	0.0057
nano-NiO						
$N$	5.4	10.0	6.1	5.0	18.3	16.8
$R$ (Å)	2.092	2.970	3.647	4.185	4.688	5.147
$\sigma^2$ (Å <sup>2</sup> )	0.0071	0.0063	0.0075	0.0104	0.0101	0.0097

of interatomic bonding occurs that requires some modification of the FF model.

We found that the original Fisher's FF model can be improved for nano-NiO by adjusting the  $\rho$  parameters of the Ni–O and O–O Buckingham potentials (Table 2), thus making both interactions more repulsive. The optimized FF model allowed us to achieve good agreement with the experimental EXAFS signal (Fig. 4) and reproduce an expansion of the nano-NiO lattice (Table 3) in agreement with the results obtained from conventional EXAFS signal analysis (Table 1).

Finally, the RDFs obtained for c-NiO and nano-NiO were analyzed by decomposition into a set of Gaussian functions. In this way, the values of structural parameters such as the coordination numbers, interatomic distances and MSRDs were obtained for the first six coordination shells (Table 3). The size effect is responsible for the variation of the coordination number with the interatomic distance: it is observed as a decrease of the ratio  $N_{\text{nano}}/N_{\text{cryst}}$  in the outer coordination shells.

Another prominent result is a change in the MSRDs. In c-NiO, the MSRD contains only a thermal disorder contribution and approaches, at large distances, a sum of the mean-squared displacements (MSD) of two atoms. The MSD values can be

experimentally determined from the diffraction experiment. For c-NiO at 300 K, they are  $\text{MSD}(\text{O}) = 0.0032 \text{ \AA}^2$  and  $\text{MSD}(\text{Ni}) = 0.0028 \text{ \AA}^2$  [27]. This means that values of the MSRDs equal to  $0.0060 \text{ \AA}^2$  and  $0.0056 \text{ \AA}^2$  are expected for Ni–O and Ni–Ni atom pairs, respectively, at large distances. These numbers are in perfect agreement with our simulation results for the fifth and sixth coordination shells (Table 3). In nano-NiO, the softening of the interaction potentials leads to a lattice expansion and to an increase of the amplitude of thermal vibrations. Besides, the distribution of structural sites contributes additionally to an increase of the MSRDs since atoms located closer to the nanoparticle surface have vibration amplitudes larger than those closer to the nanoparticle center. As a result, the average MSRDs in the nearest shells increase in nano-NiO by about  $0.002\text{--}0.004 \text{ \AA}^2$  compared to c-NiO (Table 3).

Finally, one should point out that our simple FF model is not able to reproduce the relaxation of the first coordination shell in nano-NiO found by the conventional analysis (Table 2).

## 5. Conclusions

The local relaxation phenomenon was studied in nano-sized (13 nm) nickel oxide (nano-NiO) by Ni K-edge X-ray absorption spectroscopy. Compared with microcrystalline nickel oxide (c-NiO), the lattice expansion in nano-NiO was observed, in agreement with other studies by EXAFS [26] and XRD [7,8]. The estimate, based on EXAFS signal analysis from the first two coordination shells (Table 1), suggests a volume expansion in nano-NiO by about 1%. At the same time, a contraction of the Ni–O bond by about 0.5% was observed in the first coordination shell. Note that a similar effect has been detected previously in NiO thin films [26].

The analysis of the full EXAFS signals in both c-NiO and nano-NiO was performed by a more sophisticated approach, based on a combination of classical molecular dynamics (MD) and ab initio multiple-scattering EXAFS theory [18]. We showed that the MD–EXAFS simulations of the Ni K-edge EXAFS signals in c-NiO and nano-NiO, based on a simple rigid-ion force-field model, provide good agreement with experiment (Figs. 3 and 4). Such an approach requires fewer parameters than conventional EXAFS analysis and allows one to account explicitly for thermal effects and many-atom distribution functions. The agreement between the experimental and calculated EXAFS signals can be used as a criterion to optimize the parameters of the force-field model.

## Acknowledgements

This work was supported by ESF Project 2009/0202/1DP/1.1.1.2.0/09/APIA/VIAA/141 and Latvian Government Research Grant No. 09.1518. The research leading to these results received funding from the European Community's Seventh Framework Programme (FP7/2007–2013) under grant agreement No. 226716 (Project I-20090071 EC).

## References

- [1] C.Q. Sun, Prog. Solid State Chem. 35 (2007) 1.
- [2] S. Tsunekawa, K. Ishikawa, Z.-Q. Li, Y. Kawazoe, A. Kasuya, Phys. Rev. Lett. 85 (2000) 3440.
- [3] M. Fukuhara, Phys. Lett. A 313 (2003) 427.
- [4] G. Li, J. Boerio-Goates, B.F. Woodfield, L. Li, Appl. Phys. Lett. 85 (2004) 2059.
- [5] A. Kossov, Y. Feldman, E. Wachtel, K. Gartsman, I. Lubomirsky, J. Fleig, J. Maier, Phys. Chem. Chem. Phys. 8 (2006) 1111.
- [6] R.N. Bhowmik, R. Ranganathan, R. Nagarajan, Phys. Rev. B 73 (2006) 144413.
- [7] L. Li, L. Chen, R. Qihe, G. Li, Appl. Phys. Lett. 89 (2006) 134102.
- [8] M. Ghosh, K. Biswas, A. Sundaresana, C.N.R. Rao, J. Mater. Chem. 16 (2006) 106.
- [9] S.J.L. Billinge, I. Levin, Science 316 (2007) 516.
- [10] J. Kawai, in: K. Tsuji, J. Injuk, R. Van Grieken (Eds.), X-ray Spectrometry: Recent Technological Advances, John Wiley & Sons, Chichester, 2004.
- [11] J.J. Rehr, R.C. Albers, Rev. Modern Phys. 72 (2000) 621.

- [12] K. Tsuji, K. Wagatsuma, K. Sugiyama, K. Hiraga, Y. Waseda, Surf. Interface Anal. 27 (1999) 132.
- [13] M. Ishii, B. Hamilton, N.R.J. Poolton, N. Rigopoulos, S. De Gendt, K. Sakurai, Appl. Phys. Lett. 90 (2007) 063101.
- [14] S. Larcheri, F. Rocca, F. Jandard, D. Pailharey, R. Graziola, A. Kuzmin, J. Purans, Rev. Sci. Instrum. 79 (2008) 013702.
- [15] M. Benfatto, C.R. Natoli, A. Filipponi, Phys. Rev. B 40 (1989) 9626.
- [16] A. Kuzmin, Physica B 208–209 (1995) 175.
- [17] V.L. Aksenov, M.V. Kovalchuk, A.Yu. Kuzmin, Yu. Purans, S.I. Tyutyunnikov, Crystallogr. Rep. 51 (2006) 908.
- [18] A. Kuzmin, R.A. Evarestov, J. Phys.: Condens. Matter 21 (2009) 055401.
- [19] S.A. Makhlof, F.T. Parker, F.E. Spada, A.E. Berkowitz, J. Appl. Phys. 81 (1997) 5561.
- [20] A.L. Ankudinov, B. Ravel, J.J. Rehr, S.D. Conradson, Phys. Rev. B 58 (1998) 7565.
- [21] A. Kuzmin, N. Mironova, J. Phys.: Condens. Matter 10 (1998) 7937.
- [22] J.D. Gale, A.L. Rohl, Mol. Simul. 9 (2003) 291.
- [23] C.A.J. Fisher, Scr. Mater. 50 (2004) 1045.
- [24] P.M. Oliver, G.W. Watson, S.C. Parker, Phys. Rev. B 52 (1995) 5323.
- [25] A. Kuzmin, Latv. J. Phys. Tech. Sci. 2 (2006) 7.
- [26] A. Kuzmin, J. Purans, A. Rodionov, J. Phys.: Condens. Matter 9 (1997) 6979.
- [27] D. Rodic, V. Spasojevic, V. Kusigerski, R. Tellgren, H. Rundlof, Phys. Status Solidi (b) 218 (2000) 527.